CONTROL OF LASER RADIATION PARAMETERS

Generation of controllable Ince – Gaussian modes in a passively *Q*-switched microchip laser under truncated decentred Gaussian beam pumping

CONTROL OF LASER RADIATION PARAMETERS https://doi.org/10.1070/QEL16865

Generation of controllable Ince–Gaussian modes in a passively *Q*-switched microchip laser under truncated decentred Gaussian beam pumping

Mingming Zhang, Shengchuang Bai, Jun Dong

Abstract. **We report a passively *Q*-switched (PQS) Nd:YAG/Cr^{4+}:YAG microchip laser pumped by a truncated decentred Gaussian beam for controllable Ince–Gaussian (IG) mode generation. $IG^e(n,n)$ modes ($n = 0, \ldots, 4$) are obtained experimentally by choosing the appropriate truncation parameter, which is defined as a ratio of the radius of the aperture to the beam waist. The $IG^e(4,4)$ mode is produced in the PQS Nd:YAG/Cr^{4+}:YAG microchip laser under decentred Gaussian beam pumping at a pump power of 2.6 W, the mode selection being achieved by reducing the truncation parameter. The threshold pump powers for different $IG^e(n,n)$ modes are theoretically calculated to illustrate the mode selection process. The pulsed $IG^e(n,n)$ ($n \geqslant 1$) mode generation with a peak power exceeding 1 kW and a nanosecond pulse width is obtained in the PQS microchip laser, which is a potential laser source for forming flexible vortex arrays for optical tweezers.**

Keywords: *Ince–Gaussian modes, microchip laser, Nd:YAG, passively Q-switched laser, Cr^{4+}:YAG.*

1. Introduction

High-order laser transverse modes have wide application prospects in the areas of optical trapping [1–3], optical communications [4] and quantum information problems [5]. Various high-order transverse modes have been obtained in solid-state lasers by changing the pump conditions or the structure of the laser cavity. The Ince–Gaussian (IG) modes are transition modes between Laguerre–Gaussian modes and Hermite–Gaussian modes [6, 7], and can be obtained by breaking the symmetry of the laser cavity [8–18]. For the first time, the IG mode was obtained experimentally by moving the output coupling mirror laterally and adding a crosshair in a solid-state laser [8]. Off-axis pumping [9–11], using opaque lines [12], and tilting pumping [13, 14] are all effective ways to break the symmetry of the laser resonator and have been used to achieve IG mode generation. The type of IG modes can be controlled by changing the position of the pump focus spot under off-axis pumping. Another way to control IG mode generation is to introduce diffraction loss by using opaque lines.

Mingming Zhang, Jun Dong Laboratory of Laser and Applied Photonics (LLAP), Department of Electronic Engineering, College of Electronic Science and Technology, Xiamen University, Xiamen 361005, China; e-mail: jdong@xmu.edu.cn;
Shengchuang Bai Department of Automation, Tsinghua University, Beijing 100084, China

Received 18 October 2018
Kvantovaya Elektronika **49** (3) 226–230 (2019)
Submitted in English

However, these two methods are designed for a plano-spherical cavity, and are difficult to work with in microchip lasers with a plane-parallel cavity. In addition, these solid-state lasers operate in continuous wave mode, the output power of these IG mode lasers is low and they are less efficient owing to the misalignment of the resonator. Due to the compact structure and short cavity length of the microchip laser, it is easy to obtain an output pulse with a narrow pulse width and a high peak power in the passively *Q*-switched (PQS) microchip laser. The IG mode pulsed lasers have been obtained in a PQS microchip laser by tilting the pump beam [15, 16], moving a circular aperture horizontally [17], or using decentred Gaussian beam pumping [18]. As we know, the orientations of IG laser modes can be controlled by selecting the crystalline orientation of an *a*-cut $Nd:YVO_4$ crystal under the tilted, linearly polarised laser diode end-pumped PQS microchip laser [16]. The ellipticity parameters of IG modes can be adjusted in a PQS microchip laser by using different decentred Gaussian beam pumping [18]. However, some special IG mode beams with unique applications are still not easy to be obtained in a PQS microchip laser. For example, a vortex array can be formed by using $IG^e(n,n)$ mode [2, 11]. The $IG^e(n,n)$ mode lasers are ideal sources for forming a vortex array because of their unique intensity distributions.

Up to now, $IG^e(n,n)$ modes have been generated randomly in solid-state lasers by using spatial light modulators, adjusting the position of the output coupler [8], off-axis pumping [2, 11] or using the opaque line in the laser cavity [12]. However, these lasers operate in continuous wave mode and require a long cavity; the output power and optical efficiency of the $IG^e(n,n)$ mode lasers are low, and high accurate control of the optical elements makes these lasers more difficult to maintain. Robust, compact, high peak power, controllable $IG^e(n,n)$ mode lasers are desired for various applications. Various IG modes have been generated in PQS microchip lasers under tilted beam pumping. Therefore, the formation of controllable $IG^e(n,n)$ modes in PQS microchip lasers is a challenge and deserves to be investigated.

In this paper, $IG^e(n,n)$ modes beams have been obtained in a Nd:YAG/Cr^{4+}:YAG PQS microchip laser pumped with a truncated decentred Gaussian beam. The order of the $IG^e(n,n)$ modes generated in the PQS microchip laser is up to 4 depending on the truncating parameter. The theoretical analysis of formation of $IG^e(n,n)$ modes in the Nd:YAG/Cr^{4+}:YAG PQS microchip laser are in good agreement with the experimental results.

2. Experiment

The decentred Gaussian pump beam has been formed by shifting a collimating lens laterally in the collimation and cou-

pling system. The intensity distribution of a decentred Gaussian beam (DGB) is expressed as [19]

$$I_{\mathrm{DGB}}(x,y,z) = \frac{2}{\pi w(z)^2}\exp\left[-2\frac{[x-x_{\mathrm{p}}(z)]^2+y^2}{w(z)^2}\right], \quad (1)$$

where $w(z)$ is the beam width and $x_{\mathrm{p}}(z)$ is the offset of the centre position of the DGB, which can be expressed as [13]

$$x_{\mathrm{p}}(z) = z\tan\left[-\frac{\Delta d}{f_1}-\frac{\Delta d(1-z_1/f_1)-\Delta d}{f_2}\right]. \quad (2)$$

Here, f_1 and f_2 are the focal lengths of the collimating lens and the focusing lens, respectively; Δd is the offset distance of the collimating lens from the light propagation direction of the laser diode; and z_1 is the distance between the two lenses.

A truncated decentred Gaussian beam (TDGB) is formed when an aperture is inserted between the collimating and focusing lenses. The distribution of the TDGB can be adjusted by changing the size of the aperture. The TDGB was used as a pump source to control the incident pump power distribution by adjusting the aperture size. We built a PQS Nd:YAG microchip laser for generating controllable IG$^{\mathrm{e}}(n,n)$ modes.

Figure 1 shows the TDGB pumped Nd:YAG/Cr^{4+}:YAG PQS microchip laser for generating various IG$^{\mathrm{e}}(n,n)$ modes. The experiment employs an 808 nm fibre-coupled laser diode with a numerical aperture of 0.22 and a core diameter of 400 μm as a pump source. Two plane-convex lenses with 8 mm focal length were used to collimate and focus the pump beam from the fibre-coupled laser diode. The length of the collimating and coupling system was set to be 70 mm. The collimating lens was shifted sideways by 0.15 mm to form a DGB. The focus spot diameter was measured to be approximately 160 μm. An aperture was placed between the two lenses and 10 mm from the collimating lens. The centre of the aperture was coincident with the centre of the focus lens.

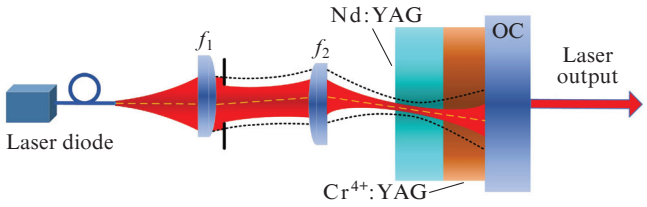

Figure 1. Experimental setup of a TDGB pumped PQS Nd:YAG/Cr^{4+}:YAG microchip laser for IG$^{\mathrm{e}}(n,n)$ mode generation.

The PQS microchip laser was formed by 1.8-mm-thick, 1 at.% doped Nd:YAG crystal, 0.5-mm-thick Cr^{4+}:YAG crystal and a plane-parallel output coupler (OC) with reflection of 95% at 1064 nm. The cavity length of microchip laser was 2.3 mm. One face of the Nd:YAG crystal was anti-reflection (AR) and high reflection (HR) coated at 808 nm and 1064 nm, respectively, to serve as the rear cavity mirror of the microchip laser. The other surface of the laser crystal was AR coated at 1064 nm to further reduce the intracavity loss. The initial transmission of the saturable absorber (SA) Cr^{4+}:YAG crystal was 95%.

3. Results and discussion

The threshold pump power for IG$^{\mathrm{e}}(n,n)$ mode PQS Nd:YAG/Cr^{4+}:YAG microchip laser can be expressed as [20–22]

$$P_{\mathrm{th}n} = \frac{\gamma_n h\nu_{\mathrm{las}}}{\eta_{\mathrm{p}}\sigma\tau L}\frac{1}{J_n(S_0,S_1,S_2,\ldots)}, \quad (3)$$

$$J_n(S_0,S_1,S_2,\ldots) = \iiint_{\mathrm{cavity}}\frac{s_{nn}(x,y,z)r_{\mathrm{p}}(x,y,z)}{1+\sum_j S_j s_{jj}(x,y,z)/I_0}\mathrm{d}x\mathrm{d}y\mathrm{d}z, \quad (4)$$

where γ_n is the total logarithmic loss per pass of the IG$^{\mathrm{e}}(n,n)$ mode; $\eta_{\mathrm{p}} = \eta_{\mathrm{t}}\eta_{\mathrm{a}}(\nu_{\mathrm{las}}/\nu_{\mathrm{p}})$; η_{t} is the optical transfer efficiency from the pump source to the gain medium; η_{a} is the absorption efficiency; ν_{las} and ν_{p} are the laser frequency and pump light frequency, respectively; L is the length of the gain medium; $r_{\mathrm{p}}(x,y,z)$ is the intracavity pump distribution; $s_{jj}(x,y,z)$ is the laser intensity distribution; $I_0 = (c\sigma\tau)^{-1}$; τ is the fluorescence lifetime; c is the light velocity in the vacuum; σ is the laser transition cross section; and S_n is the photon number of the IG$^{\mathrm{e}}(n,n)$ mode in the cavity.

The truncation parameter is defined as $\beta = a/w_{\mathrm{a}}$, where a is the radius of the circular aperture, and w_{a} is the beam width of the pump beam incident on the aperture. Therefore, the TDGB pump power distribution can be described as

$$r_{\mathrm{p}}(x,y,z) = \frac{2}{\pi w_{\mathrm{p}}(z)^2}\exp\left\{-2\frac{[x-x_{\mathrm{p}}(z)]^2+y^2}{w_{\mathrm{p}}(z)^2}-\alpha z\right\} \times H(\beta w_{\mathrm{p}}(z)-\sqrt{[x-x_{\mathrm{p}}(z)]^2+y^2}), \quad (5)$$

where H is the Heaviside step function, $w_{\mathrm{p}}(z)$ is the beam width of the decentred pump beam, and α is the absorption coefficient of the gain crystal. Here, $\beta \geqslant 0.4$, and hence the effect of the aperture on the diffraction of the pump beam is negligible.

The IG mode is divided into even and odd modes, which are denoted by the superscripts e and o, respectively. The electric field expressions of the IG modes can be expressed as [6, 7]

$$\mathrm{IG}^{\mathrm{e}}_{pm}(r,\varepsilon) = C_0 C_p^m(\mathrm{i}\xi,\varepsilon)C_p^m(\eta,\varepsilon)\exp\left[-\frac{r^2}{w_{\mathrm{las}}(z)^2}\right] \times\exp\mathrm{i}\left[kz+\frac{kr^2}{2R(z)}-(p+1)\psi_z(z)\right], \quad (6)$$

$$\mathrm{IG}^{\mathrm{o}}_{pm}(r,\varepsilon) = S_0 S_p^m(\mathrm{i}\xi,\varepsilon)S_p^m(\eta,\varepsilon)\exp\left[-\frac{r^2}{w_{\mathrm{las}}(z)^2}\right] \times\exp\mathrm{i}\left[kz+\frac{kr^2}{2R(z)}-(p+1)\psi_z(z)\right], \quad (7)$$

where C_0 and S_0 are normalisation constants; $x = f(z)\times\cosh\xi\cos\eta$ and $y = f(z)\sinh\xi\sin\eta$ are the elliptic coordinates; $\eta \in [0,\infty)$ and $\eta \in [0,2\pi)$ are the radial and the angular elliptic variables, respectively; $C_p^m(\cdot,\varepsilon)$ and $S_p^m(\cdot,\varepsilon)$ are the even and odd Ince polynomials of order p and degree m, respectively; $\varepsilon = 2f_0^2/w_0^2$ is the ellipticity parameter; $f(z) = f_0 w(z)/w_0$; f_0 is the semifocal separation at the waist plane $z = 0$; $R(z)$ is the

radius of curvature of the phase front; $\Psi_z(z) = \arctan(z/z_R)$; and z_R is the Rayleigh length.

For the $IG^e(n,n)$ laser modes obtained in the microchip laser, the laser intensity distribution $s_{nn}(x,y,z)$ is given by

$$s_{nn}(x,y,z) = \left| IG^e_{nn}(x,y,z) \right|^2. \tag{8}$$

Therefore, the threshold pump power of the fundamental mode is calculated by the formula [20]

$$P_{th0} = \frac{\gamma_n h\nu_{las}}{\eta_p \sigma \tau L} \frac{1}{J_0(0,0,0,...)}. \tag{9}$$

Higher-order modes need to beat adjacent low-order modes to oscillate in the cavity. The threshold pump power of the $IG^e(n,n)$ mode is calculated by numerically solving the nonlinear equations for P_{thn}

$$J_{n-1}(...,0,S_{n-1},0,...) = \frac{\gamma_{n-1} h\nu_{las}}{\eta_p \sigma \tau L} \frac{1}{P_{thn}}, \tag{10}$$

$$J_n(...,0,S_{n-1},0,...) = \frac{\gamma_n h\nu_{las}}{\eta_p \sigma \tau L} \frac{1}{P_{thn}}. \tag{11}$$

We can use Eqns (9)–(11) to estimate the threshold pump power of the $IG^e(n,n)$ mode generated by a TDGB pumped PQS Nd:YAG/Cr^{4+}:YAG microchip laser.

The output laser transverse intensity distributions of the PQS Nd:YAG/Cr^{4+}:YAG microchip laser for different truncation parameters were measured at the incident pump power of 2.6 W, as shown in Fig. 2. When the truncation parameter β was large than 0.85, the $IG^e(4,4)$ mode was obtained. As the radius of the aperture decreases, the truncation parameter β decreases accordingly, the $IG^e(n,n)$ mode oscillation being maintained in the PQS Nd:YAG/Cr^{4+}:YAG microchip laser. However, the order of the $IG^e(n,n)$ modes generated in the microchip laser decreases. The effective pump area inside the gain medium was decreased by reducing the aperture radius, and the achievable gain distribution inside the gain medium is not sufficient to support high order mode oscillation; therefore, the order of the $IG^e(n,n)$ mode decreases with decreasing β. For instant, the stable $IG^e(3,3)$ mode was oscillated when $\beta = 0.8$, and the $IG^e(2,2)$ mode and $IG^e(1,1)$ mode are generated when $\beta = 0.7$ and 0.6, respectively. When the radius of the aperture is further reduced to 0.5, the available gain area is further reduced and is not sufficient to support high-order mode oscillation, and only the fundamental mode is oscillating. When $\beta < 0.43$, there is no laser output generated in the microchip laser. This is caused by a rapid decrease in the pump power incident on the gain medium and by an increase in the diffraction loss owing to the tiny aperture. A large pump beam area with sufficient pump power intensity is required for high-order mode oscillation in the microchip laser cavity. Different stable $IG^e(n,n)$ mode oscillation in the PQS Nd:YAG/Cr^{4+}:YAG microchip laser is achieved by adjusting the radius of the aperture. Therefore, desirable $IG^e(n,n)$ modes can be obtained in the microchip laser by simply adjusting the beam size of the DGB. The theoretically calculated IG mode distributions based on the even IG mode expression are shown in Fig. 3, which are in good agreement with the experimentally obtained results.

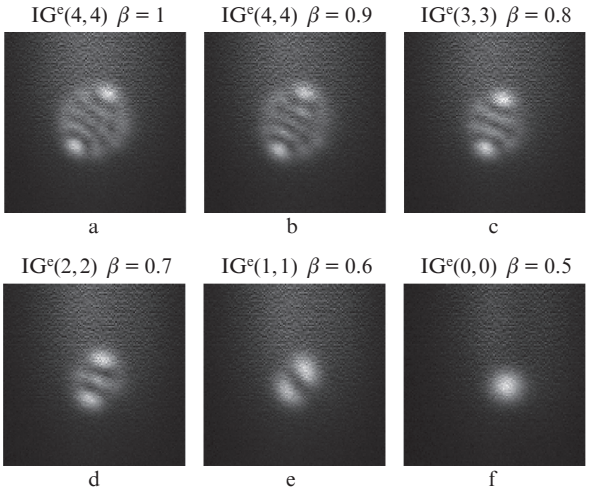

Figure 2. Variation of the laser transverse mode distribution observed in the PQS Nd:YAG/Cr^{4+}:YAG microchip laser with the change in the truncation parameter β.

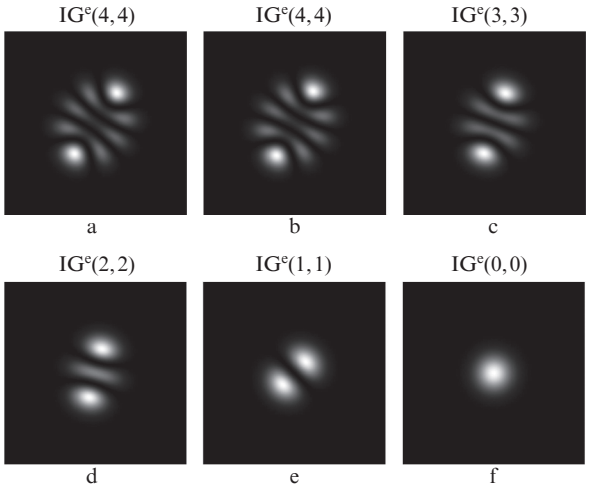

Figure 3. Numerically reconstructed IG mode distributions with the ellipticity parameter $\varepsilon = 3$, which correspond to the experimentally obtained $IG^e(n,n)$ mode transverse distributions for different β in Fig. 2.

The threshold pump powers of different $IG^e(n,n)$modes are calculated by numerically solving the nonlinear coupled equations (9)–(11). Figure 4 presents the theoretically calculated threshold pump powers of four $IG^e(n,n)$ modes as functions of the truncation parameter β; the threshold pump power of the TEM_{00} fundamental mode is also shown for comparison. Curves (*1–5*) correspond to the threshold pump powers for TEM_{00}, $IG^e(1,1)$, $IG^e(2,2)$, $IG^e(3,3)$ and $IG^e(4,4)$ modes, respectively. The parameters used in the theoretical calculation are as follows: $\sigma = 2.8 \times 10^{-19}$ cm^2, $L = 1.8$ mm, $R_{OC} = 95\,\%$, $\alpha = 7.8$ cm^{-1}, $\gamma_0 = 0.11$, $\gamma_1 = 0.12$, $\gamma_2 = 0.13$, $\gamma_3 = 0.14$, $\gamma_4 = 0.15$, $\tau = 230$ μs, $w_p(0) = 80$ μm, and $w_{las}(0) = 80$ μm. The threshold pump power of the $IG^e(n,n)$ mode rises as the truncation parameter decreases. The threshold pump power increases with the order of the IG mode when the truncation parameter is fixed. From Fig. 4, we can see that the threshold pump power of TEM_{00} mode is the lowest for different truncation parameters β.

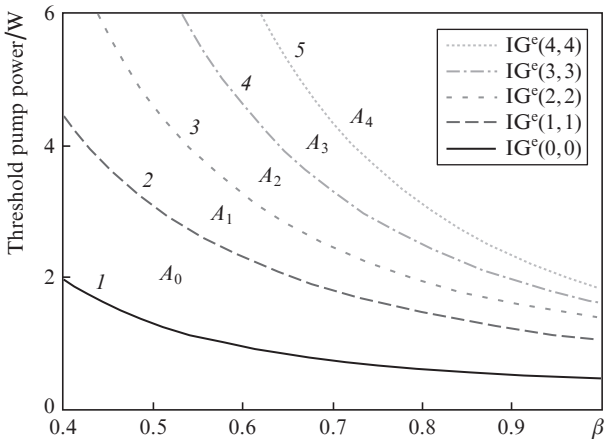

Figure 4. Theoretically calculated threshold pump powers of the $IG^e(n,n)$ modes vs. truncation parameter β.

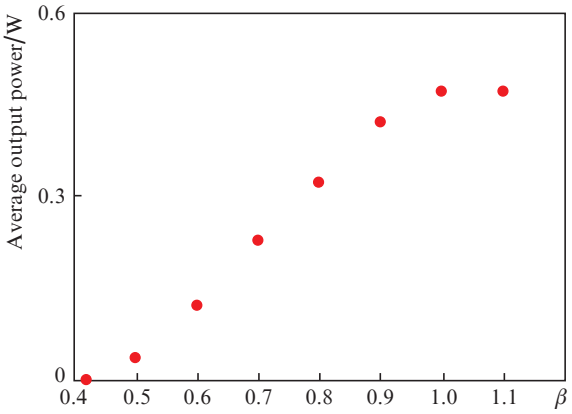

Figure 5. Average output power as a function of the truncation parameter.

Note that while the threshold pump power of $IG^e(1,1)$ mode is higher than that of the TEM_{00} mode, the $IG^e(1,1)$ mode prefers to oscillate when the pump power is higher than the threshold pump power of $IG^e(1,1)$ mode. This fact can be explained by the advantage of the $IG^e(1,1)$ mode over the TEM_{00} mode with respect to the gain competition. The stable domain A_0 of the TEM_{00} mode generation is enclosed between curves (*1*) and (*2*). The $IG^e(1,1)$ mode is stable in region A_1 enclosed between curves (*2*) and (*3*). The $IG^e(2,2)$ mode is stable in region A_2 between curves (*3*) and (*4*), while the $IG^e(3,3)$ mode is stable in region A_3 enclosed between curves (*4*) and (*5*). The $IG^e(4,4)$ mode is oscillated in region A_4 beyond curve (*5*).

When the incident pump power P_{in} from the fibre-coupled laser diode is fixed at 2.6 W, stable $IG^e(n,n)$ modes with n from 1 to 4 are obtained by gradually changing the truncation parameter β. When $\beta = 0.5$, the incident pump power is higher than the threshold pump power of the TEM_{00} mode and lower than the threshold power of the $IG^e(1,1)$ mode. Therefore, only the TEM_{00} mode was obtained under this pump condition. Higher-order IG modes will be oscillated in the cavity with the further increase in the truncation parameter. When the truncation parameters are 0.6, 0.7, 0.8 and 0.9, respectively, the pump conditions satisfy the oscillation thresholds of the $IG^e(1,1)$, $IG^e(2,2)$, $IG^e(3,3)$ and $IG^e(4,4)$ modes, respectively.

From Fig. 4, we can see that distinct $IG^e(n,n)$ mode generation can be obtained by adjusting the pump power at $\beta = 1$ (DGB pump case) because the effect of the aperture size on the pump beam is negligible at $\beta \geqslant 1$. However, the threshold pump powers of the $IG^e(n,n)$ modes with different orders are relatively close, and it is difficult to select $IG^e(n,n)$ mode with the desired order. Also, the output power for the $IG^e(n,n)$ mode laser with $n < 4$ is limited owing to the narrow pump power range for mode transition. The pump power range increases with decreasing β as shown in Fig. 4. Therefore, it is easy to control the order of the $IG^e(n,n)$ mode in a TDGB pumped PQS microchip laser with small β compared to a DGB pumped PQS microchip laser.

Figure 5 shows the variation of the average output power as a function of the truncation parameter when $P_{in} = 2.6$ W. The average output power remains unchanged at $\beta > 1$. Meanwhile, the output mode is always the $IG^e(4,4)$ mode at $\beta > 1$, which indicates that the effect of the aperture on the laser mode is negligible in this case. When $\beta < 1$, the average output power decreases near linearly with decreasing β. When $\beta < 0.43$, there is no laser mode generated in the microchip laser. A maximum average output power of 470 mW was obtained for the $IG^e(4,4)$ mode at $\beta > 1$.

The repetition rate, pulse width, pulse energy and peak power as functiond of the truncation parameter are shown in Fig. 6. The repetition rate is kept at about 30 kHz when $\beta > 0.9$, and then decreases slowly when $\beta < 0.9$. The pulse width is maintain around 6 ns and almost independent of β. When $\beta > 1$, the pulse energy and the peak power remain unchanged around 15.8 μJ and 2.5 kW, respectively. While both the pulse energy and the peak power decrease with decreasing β (down

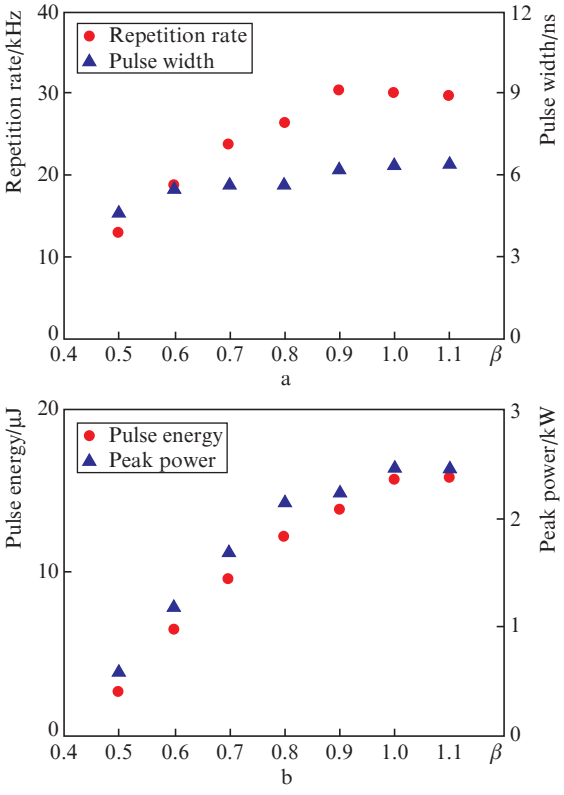

Figure 6. (a) Repetition rate and pulse width and (b) pulse energy and peak power as functions of the truncation parameter.

to $\beta < 1$), the $IG^e(n,n)$ mode ($n \geqslant 1$) generation with a peak power exceeding 1 kW has been achieved in the PQS microchip laser.

4. Conclusions

A truncated decentred Gaussian pump beam has been successfully used to control the $IG^e(n,n)$ mode generation in the PQS Nd:YAG/Cr^{4+}:YAG microchip laser. The $IG^e(1,1)$, $IG^e(2,2)$, $IG^e(3,3)$ and $IG^e(4,4)$ modes have been obtained by adjusting the truncation parameter in the PQS microchip laser. The $IG^e(n,n)$ mode ($n \geqslant 1$) laser pulses with a peak power exceeding 1 kW and a nanosecond pulse width have been generated in the PQS microchip laser. The theoretically calculated threshold pump powers for different $IG^e(n,n)$ mode lasers as a function of the truncation parameter provide a clear insight into mode selection in a PQS microchip laser. The $IG^e(n,n)$ mode controllable Nd:YAG/Cr^{4+}:YAG PQS microchip laser with a nanosecond pulse width and a high peak power are potential laser sources for forming pulsed vortex arrays consisting of $n \times n$ embedded optical vortexes, which can be used in optical trapping and quantum information processing applications.

Acknowledgements. This work was supported by the National Natural Science Foundation of China (Grant Nos 61475130, 61275143), and the Programme for New Century Excellent Talents in University (Grant No. NCET-09-0669).

References

1. Woerdemann M., Alpmann C., Denz C. *Appl. Phys. Lett.*, **98** (11), 111101 (2011).
2. Kuo C.F., Chu S.C. *Opt. Express*, **21** (22), 26418 (2013).
3. Chen Y.J., Zigo S., Raithel G. *Phys. Rev. A*, **89** (6), 063409 (2014).
4. Trichili A., Ben Salem A., Dudley A., Zghal M., Forbes A. *Opt. Lett.*, **41** (13), 3086 (2016).
5. Krenn M., Fickler R., Huber M., Lapkiewicz R., Plick W., Ramelow S., Zeilinger A. *Phys. Rev. A*, **87** (1), 012326 (2013).
6. Bandres M.A., Gutierrez-Vega J.C. *Opt. Lett.*, **29** (2), 144 (2004).
7. Bandres M.A., Gutierrez-Vega J.C. *J. Opt. Soc. Am. A*, **21** (5), 873 (2004).
8. Schwarz U.T., Bandres M.A., Gutierrez-Vega J.C. *Opt. Lett.*, **29** (16), 1870 (2004).
9. Chu S.C. *Opt. Express*, **15** (25), 16506 (2007).
10. Malyutin A.A. *Quantum Electron.*, **37** (3), 299 (2007) [*Kvantovaya Elektron.*, **37** (3), 299 (2007)].
11. Ohtomo T., Chu S.C., Otsuka K. *Opt. Express*, **16** (7), 5082 (2008).
12. Lei J., Hu A., Wang Y., Chen P. *Appl. Phys. B*, **117** (4), 1129 (2014).
13. Ohtomo T., Kamikariya K., Otsuka K., Chu S.C. *Opt. Express*, **15** (17), 10705 (2007).
14. Otsuka K., Nemoto K., Kamikariya K., Miyasaka Y., Chu S.C. *Jpn. J. Appl. Phys.*, **46** (9A), 5865 (2007).
15. Dong J., Ma J., Ren Y.Y., Xu G.Z., Kaminskii A.A. *Laser Phys. Lett.*, **10** (8), 085803 (2013).
16. He H.S., Zhang M.M., Dong J., Ueda K.I. *J. Opt.*, **18** (12), 125202 (2016).
17. Han S., Liu Y.Q., Zhang F., Zhou Y., Wang Z.P., Xu X.G. *IEEE Photonics J.*, **7** (1), 4500206 (2015).
18. Zhang M.M., He H.S., Dong J. *IEEE Photonics J.*, **9** (2), 1501214 (2017).
19. Alrashed A.A.R., Saleh B.E.A. *Appl. Opt.*, **34** (30), 6819 (1995).
20. Kubodera K.i., Otsuka K. *J. Appl. Phys.*, **50** (2), 653 (1979).
21. Chen Y.F., Lan Y.P., Wang S.C. *Appl. Phys. B*, **72** (2), 167 (2001).
22. Qiao Z., Kong L.C., Xie G.Q., Qin Z.P., Yuan P., Qian L.J., Xu X.D., Xu J., Fan D.Y. *Opt. Lett.*, **42** (13), 2547 (2017).